PAPER • **OPEN ACCESS**

Functionalized nanodiamonds – toward innovative antitumor approaches

To cite this article: Marta Boreggio *et al* 2026 *Nano Ex.* **7** 015008

IOP Publishing Nano Express 7 (2026) 015008 https://doi.org/10.1088/2632-959X/ae378a

NANO EXPRESS

OPEN ACCESS

RECEIVED
2 October 2025

REVISED
22 December 2025

ACCEPTED FOR PUBLICATION
13 January 2026

PUBLISHED
27 January 2026

PAPER

Functionalized nanodiamonds – toward innovative antitumor approaches

Marta Boreggio[1], Elena Rosini[2], Filippo Moncalvo[1], Tana Zavodna[3], Sarka Hradilova[3], Francesco Cellesi[1], Loredano Pollegioni[2], Katerina Polakova[3,*] and Elisa Fasoli[1,*]

[1] Dipartimento di Chimica, Materiali e Ingegneria Chimica 'Giulio Natta', Politecnico di Milano, Via Mancinelli 7, 20131, Milano, Italy
[2] Dipartimento di Biotecnologie e Scienze Molecolari Università degli Studi dell'Insubria, Via J.H. Dunant 3, 21100 Varese, Italy
[3] Czech Advanced Technology and Research Institute, Slechtitelu 241/27, 77900 Olomouc-Holice, Czechia
[*] Authors to whom any correspondence should be addressed.

E-mail: katerina.polakova@upol.cz **and** elisa.fasoli@polimi.it

Keywords: D-amino acid oxidase, drug delivery, nanodiamonds, cytotoxicity, protein corona, mass spectrometry

Supplementary material for this article is available online

Abstract

D-amino acid oxidase (DAAO) represents a promising and well-characterized enzyme for the 'enzyme-activated prodrug therapy', one of the newest frontiers for anticancer treatment. This flavoprotein catalyzes the deamination of D-amino acids with production of hydrogen peroxide, a reactive oxygen species (ROS) able to favor cells death. In this preliminary work, promising drug delivery systems based on nanodiamonds (NDs) were designed to target DAAO specifically to the tumor site following possible future injection in the blood stream. NDs were functionalized with polyethylene glycol (PEG), hyaluronic acid (HA) and poly(glycerol monomethacrylate) (PGMA), to reduce aggregation and improve biocompatibility. Different conjugates were obtained by DAAO adsorption on the NDs surface. The interaction with human serum proteins was evaluated *in vitro*, and the formation of the protein corona (PC) was investigated via nLC-MS/MS, aiming to characterize both soft and hard corona. Because the PC provides a biological identity to the conjugates and influences their fate *in vivo*, this study may contribute to investigate preliminary *in vitro* properties of functionalized nanoparticles, conjugated with well-characterized enzyme. The cytotoxicity and the oxidative stress of the designed conjugates, induced by hydrogen peroxide, were tested on two different tumor and two different healthy cell lines, as controls. The contribution of the PC to both cytotoxicity and oxidative stress was also evaluated. Among all investigated NDs-DAAO conjugates, PEG-NDs-DAAO seemed to exhibit promising antitumor characteristics: a biocompatible PC may contribute to potentially prolong blood circulation time and the increased cytotoxicity against human breast cancer cells (SKBR3, viability of 34%) could be probably favored by interaction of PEG-NDs-DAAO-PC with tumor cells. The presence of specific proteins, like serotransferrin and Inter-alpha-trypsin inhibitor heavy chain H2, could potentially play a crucial role in cell membrane adhesion.

1. Introduction

The enzyme-activated prodrug therapy (EPT), one of the newest anticancer frontiers, consists of a two-step approach. Firstly, a drug-activating enzyme is targeted to the tumor site. Then, a nontoxic prodrug, which acts as the enzyme's substrate, is administered systemically and converted into an active anticancer drug specifically in the tumor by the enzyme [1]. D-amino acid oxidase (DAAO, EC 1.4.3.3) from the yeast *Rhodotorula gracilis* is a promising and well-characterized enzyme for an EPT application. It catalyzes the oxidation of the prodrugs D-amino acids into the corresponding α-keto acids, ammonia and hydrogen peroxide (H_2O_2) [2]. The overproduction of H_2O_2 inside the tumor site induces a cytotoxic effect, damaging DNA, proteins and lipids [3].

The very low endogenous concentration (micromolar to sub-millimolar range) of D-amino acids in human body, mainly originating from gut microbiota and foods, allows easier regulation of the enzyme activity in therapy [4, 5]. The DAAO specificity for D-amino acids and its broad reported knowledge in terms of kinetics, H_2O_2 production and enzyme's turnover, have guided the choice of DAAO to design possible nanocarriers devoted to target enzyme in the tumor tissue.

In addition, few studies conjugated DAAO with nanoparticles (NPs), like iron oxide and gold NPs and multi-walled carbon nanotubes, all reporting a higher stability of DAAO after conjugation [6, 7]. In this context, nanodiamonds (NDs), 3D carbon allotropes, are of particular interest because of their high biocompatibility and adsorption capacity, and easy functionalization [8]. Moreover, different studies highlighted a lower cytotoxicity than the other carbonaceous nanomaterials, due to a lower generation of cytotoxic reactive oxygen species (ROS) [9]. The coupling of DAAO with NDs is expected to improve DAAO stability and bioavailability, and to prolong its retention time within the tumor due to the Enhanced Permeability and Retention (EPR) effect, increasing its therapeutic efficacy [10]. Once systemically administered, NPs interact with blood components, especially plasma proteins, that instantly create a protein layer around NPs' surface, called protein corona (PC) or bio-corona [11]. The PC is composed by a primary inner layer of tightly almost irreversibly bound proteins generated by direct protein-NPs interaction, called hard corona (HC), and an outer more loosely bound layer composed by proteins that interact with the HC via protein–protein interactions, called soft corona (SC) [12]. As the PC gives the NPs a biological identity influencing their fate *in vivo*, its investigation is crucial [13]. For instance, the presence of dysopsonins (e.g., albumin and apolipoproteins (Apos)) in the PC, could prolong the NPs' circulation time, favoring NPs' recognition as 'self'-structures, while opsonins (e.g., fibronectin and immunoglobulins (Igs)) could contribute to phagocytosis, quickly removing the nanosystems and preventing them the reach their target tissue [14]. The PC formation is connected to the physicochemical properties of NPs, including surface properties (e.g., chemistry, charge, roughness etc), size and shape. These properties influence the amount and the type of proteins constituting the PC [15]. Recently, many research works focused on the modification of NDs' surface by different biocompatible polymers in order to generate a more performant PC, in terms of biocompatibility and biodistribution, and to reduce the NDs' aggregation in biological fluids [16].

Using polyethylene glycol (PEG), one of the most studied polymers, researchers created stealth drug carriers with prolonged circulation time, reducing NPs' recognition and clearance by the mononuclear phagocyte system [17]. Moreover, previous studies demonstrated that the coupling of DAAO with PEG favored the enzyme's stability, thus increasing its therapeutic efficacy [18]. NPs' functionalization with hyaluronic acid (HA) reduced both the protein adsorption and the rate of macrophages' uptake. The HA association with NDs for tumor imaging and therapy was recently highlighted, for its ability to increase the CD44 receptors mediated phagocytosis of NPs in many cancer cell lines [19]. Synthetic poly(glycerol monomethacrylate) (PGMA), obtained by Atom Transfer Radical Polymerization (ATRP), is the subject of ongoing research for its ability to reduce both the NPs' interaction with physiological proteins and to activate the immune system [20–22].

Our research is aimed to optimize the design of promising antitumor nanosystems by NDs' functionalizion with PEG, HA or PGMA, and conjugation with DAAO (f-NDs-DAAO) [2, 23]. To compare the effects of the selected functionalization molecules on the behavior of the NDs conjugates, the following *in vitro* formulation screenings were carried out. The cytotoxicity and the oxidative stress, induced by H_2O_2, were evaluated on different cell lines, like immortalized human cervical cancer cells (HeLa) and breast cancer cells (SKBR3), as well as on mouse embryonic fibroblasts (NIH3T3) and human lung fibroblasts (HEL), used as non-cancerous controls. Moreover, the cellular uptake of f-NDs-DAAO was investigated via flow cytometry, and the PC composition after incubation in human serum was investigated using a proteomic approach based on electrophoretic separation (SDS-PAGE) and mass spectrometry (nLC-MS/MS). The influence of the PC on the cytotoxicity against the selected cell lines was evaluated, also considering recent studies demonstrating how PC could enhance the cytotoxic effect [24, 25]. PEG-NDs-DAAO seemed to exhibit a combination of biocompatible PC and increased cytotoxic effect against human breast cancer cells (SKBR3).

2. Materials and methods

2.1. Design of NDs

Carboxylated NDs (COOH-NDs) and all reagents were purchased from Merck Millipore® and they were used without any further purification.

2.1.1. NDs functionalization with HA

For the functionalization of COOH-NDs with HA (8–15 kDa), a two-step procedure was applied. The first step consists in the amidation of NDs' surface. In the second step, HA polymer chains are covalently attached on amidated NDs' surface.

In detail, 100 mg of COOH-NDs were mixed with 13 ml ethylene diamine, 626 mg N-ethyl-N′-(3-dimethylaminopropyl)carbodiimide hydrochloride (EDC HCl), and 376 mg N-hydroxysuccinimide (NHS) in an iced bath until dissolution. Then, 450 μl triethylamine was added drop by drop and left under stirring for 4 days at room temperature, followed by centrifugation (21000 x g for 10 min) and washed with 10 ml acetone until neutral pH. The obtained amidated NDs (NH_2-NDs) were then dried at 90 °C overnight.

50 mg of NH_2-NDs were mixed with 10 mg HA, 156 mg EDC HCl, 94 mg NHS and 5 ml formamide, and sonicated for 10 min at room temperature. Then, 113 μl triethylamine was added drop by drop and left under stirring for a week at room temperature, followed by centrifugation (21000 x g for 10 min) and washed with 10 ml acetone until neutral pH. The obtained NDs functionalized with HA (HA-NDs) were then dried at 90 °C overnight and characterized by thermal gravimetric analysis (TGA) (heating from 35 to 900 °C in air), to evaluate the functionalization degree.

2.1.2. NDs functionalization with PEG

100 mg of COOH-NDs were mixed with 14 mg PEG (5 kDa), 6 mg N,N′-dicyclohexylcarbodiimide (DCC) and 2 mg 4-dimethylaminopyridine (DMAP), and sonicated for 2 h at room temperature. Then, the reaction mixture was left under stirring for 6 days at room temperature. The obtained samples were centrifuged (21000 x g for 10 min) and washed 10 times with 10 ml N,N-dimethylformamide (DMF) and 10 times with 10 ml methanol. The obtained PEGylated NDs (PEG-NDs) were then dried at 90 °C overnight and characterized with TGA, to evaluate the functionalization degree.

2.1.3. NDs functionalization with PGMA

The functionalization of COOH-NDs with PGMA was obtained through a three-step procedure.

Firstly, amidation of COOH-NDs was performed, following the same procedure reported in paragraph 2.1.1, to obtain NH_2-NDs. The second step consists in the covalent attachment of α-bromoisobutyryl bromide (BiBB), to obtain grafted ATRP initiators on the surface of NDs. Briefly, 50 mg of NH_2-NDs were dispersed in 50 ml of DMF by sonication at room temperature for 15 min and left under nitrogen atmosphere performing three vacuum/nitrogen cycles. Then, 2.5 ml triethylamine were added dropwise and the solution was kept under stirring for 10 min. 2.25 ml of BiBB in 25 ml DMF were dropped into the reaction mixture, which was kept under stirring and nitrogen atmosphere at room temperature for 24 h. The obtained sample (Br-NDs) was then centrifuged (21000 x g for 10 min), washed 5 times with 10 ml acetone, 5 times with 10 ml ethanol, and 5 times with 10 ml water and dried at 90 °C overnight.

In the final step, aqueous Activators ReGenerated by Electron Transfer (ARGET) ATRP was adapted from a previous protocol [21, 22], to polymerize PGMA from Br-NDs. Briefly, 5 mg of Br-NDs were sonicated for 5 min with 200 mg glycerol monomethacrylate (GMA, 160.20 g/mol, 1.25 mmol) and 7.6 ml of degassed 100 mM phosphate-buffered saline (1x PBS) and the reaction mixture was left under nitrogen atmosphere performing three vacuum/nitrogen cycles. Then, 30 μl copper (II) chloride ($CuCl_2$, 0.75 μmol), Tris(2-pyridylmethyl)amine (TPMA, 6 μmol) from $CuCl_2$/TPMA stock solution in 1x PBS ($CuCl_2$ 25 mM, TPMA 200 mM, [$CuCl_2$]/[TPMA] 1:8 mol/mol) and 100 μl DMF (used as ^{1}H -NMR peak reference) were added, and the resulting solution was purged with nitrogen for further 5 min. 15 μL of 8 mM ascorbic acid (AscA) stock solution in 1x PBS were added to the reaction mixture every 15 min, which was kept under stirring for 7 h at 30 °C. Samples (150 μL) were withdrawn at different time intervals for ^{1}H NMR analysis to monitor the polymerization and molecular weight. The resulting NDs functionalized with PGMA (PGMA-NDs) were centrifuged (21000 x g for 10 min) and washed 10 times with 10 ml water and 10 times with 10 ml acetone. Following drying at 90 °C overnight, NDs were characterized by TGA and Fourier-transform infrared spectroscopy (FTIR).

2.2. NDs functionalization with DAAO

The recombinant His-DAAO wild-type was expressed and purified from BL21(DE3)pLysS *E. coli* cells as described by Fantinato *et al* [26]. The pure enzyme had a specific activity on D-alanine (D-Ala) of 115 U/mg protein at 25 °C, with > 90% purity as confirmed by SDS-PAGE analysis. The absorbance spectrum of a properly diluted enzyme sample aliquot was used to measure the enzyme concentration ($\varepsilon_{455nm} = 12.6\ mM^{-1}\ cm^{-1}$) [27].

A suspension of 2 mg of HA-NDs was sonicated for 2 h at room temperature in 400 μl of 50 mM sodium pyrophosphate buffer (pH 7.4). The suspension was incubated overnight in 1.5 ml of a 2 mg ml^{-1} DAAO solution, using a rotating plate at 4 °C with a gentle stirring. The produced adduct (HA-NDs-DAAO) was separated

from the supernatant, containing unbound DAAO, by centrifugation (420 x g) for 5 min at room temperature. To remove any trace of dispersed NDs, supernatant was collected and centrifuged (12200 x g, at room temperature) four times for 5 min, recovering the solution, following our standardize protocol [6]. It was then stored for further analysis.

The same procedure was applied also to PEG-NDs and PGMA-NDs, to obtain PEG-NDs-DAAO and PGMA-NDs-DAAO conjugates, respectively.

All the obtained adducts were characterized by Dynamic Light Scattering (DLS) to determine particles' hydrodynamic size and zeta potential, using a Zetasizer Nano ZS (Malvern Instrument). The samples were measured at room temperature at a concentration of 0.05 mg ml^{-1} and a total volume of 2 ml, in a disposable transparent cuvette. The colloidal stability of f-NDs-DAAO was investigated in 1x PBS.

2.3. DAAO activity and stability assay

The activity of all f-NDs-DAAO samples was determined using the horseradish peroxidase (EC 1.11.1.7; Roche®) and *o*-dianisidine (Merck Millipore®) coupled assay [28]. In detail, the assay was performed at the final concentration of 0.1 mg ml^{-1} for both HA-NDs-DAAO and PEG-NDs-DAAO, and of 0.3 mg ml^{-1} for PGMA-NDs-DAAO. The analyses were replicated three times for each assay and the mean ± standard deviation (SD) was calculated.

The stability of different conjugates at 37 °C was assayed measuring the residual activity of the enzyme, every 60 min for the first four hours and then at 24 h of incubation under gentle stirring. The activity value at 0 h for each sample was taken as 100%.

2.4. Protein corona investigation

2.4.1. Incubation of f-NDs-DAAO in human serum

2 mg of HA-NDs-DAAO, PEG-NDs-DAAO and PGMA-NDs-DAAO were suspended in 100 μl of 1x PBS pH 7.4, and incubated with 1900 μl of human serum (HS) (Merk Millipore®) at 37 °C for 4 h, under gentle stirring [29]. The obtained f-NDs-DAAO-PCs (i.e., HA-NDs-DAAO-PC, PEG-NDs-DAAO-PC and PGMA-NDs-DAAO-PC) were recovered from HS supernatant by gentle centrifugation (45 x g for 30 s). PCs were then eluted three times using 500 μl 1x PBS solution at 37 °C (E1), 500 μl 1x PBS solution at 37 °C (E2), and 500 μl 20 mM dithiothreitol (DTT) solution at 99 °C (E3). Each elution step was performed for 10 min under vigorous stirring. Elutions E1 and E2 detached SC's proteins, while E3 was used to collect HC's proteins.

2.4.2. SDS-PAGE and mass spectrometry

The protein concentration of eluates E1 was evaluated with the Pierce™ Bicinchoninic Acid Protein Assay kit (BCA, Thermo Scientific), using bovine serum albumin as standard. The protein content of both eluates E2 and E3 was not quantified: E2 was used as a washing step to remove the remaining SC proteins not eluted with E1, E3 contained an amount of DTT not compatible with the kit.

SDS-PAGE analysis was as stated in Boreggio *et al* [6]. All the eluates were treated under native conditions (solubilized in 4x Laemmli buffer at room temperature) and they were loaded onto SDS-PAGE gels as following: 100 μl of E1, 500 μl of E2 and 500 μl of E3 for all f-NDs-DAAO. All gels were cut and treated following the standardized protocols, using trypsin as digestive enzyme [6].

8 μl of tryptic-digested samples were injected in a nanochromatography system (UltiMate 3000 RSLCnano System, Thermo Scientific), coupled with a mass spectrometer (LTQ XL, Thermo Scientific). The mass spectrometry (MS) data were analyzed by the Mascot search engine (Version 2.3.01), using the Proteome Discoverer software (v. 1.2.0 Thermo) and consulting specific UniProtKB/Swiss-Prot protein database (Swiss-Prot_HomoSapiens 42,390 sequences and 24,374,355 residues). A preliminary subtraction of common contaminants was performed using definite *Contaminants* database (14,935 sequence, 5,081,069 residues). The serum proteins, identified in the bio-corona of f-NDs-DAAO were compared by Venn diagram (https://bioinfogp.cnb.csic.es/tools/venny/). UniProtKB database (https://www.uniprot.org) was used to evaluate the biological processes of the identified serum proteins.

All E1 eluates were loaded on SDS-PAGE gel and analyzed by mass spectrometer four times to obtain technical replicates. The data validation was performed considering only proteins recognized in all replicates as reliable identifications. E2 was considered as a washing step, and E3 was analyzed only once because of low amount of proteins. In Supplementary File S1, the list of the four technical replicates of E1, of validated proteins of E1 (list of the SC's proteins), and of proteins belonging to the HC (identifications in E3) for f-NDs-DAAO, are reported.

2.5. *In vitro* cytotoxicity assay and ROS measurement

The cytotoxicity and the production of ROS by f-NDs-DAAOs was assessed in human HeLa (immortalized cervical cancer, ATCC CCL-2, Manassas, VA, USA) and human SKBR3 (breast carcinoma, ATCC HTB-30, Manassas, VA, USA) cancer cell lines, as well as in human fibroblast HEL 12469 (embryonic, lung, ECACC, Salisbury, UK) and mouse fibroblast NIH3T3 (embryonic, ATCC CRL-1658, Manassas, VA, USA) cells, as healthy controls, using the LIVE/DEAD cytotoxicity/viability test (Invitrogen) and the oxidative stress indicator CM-H2DCFDA (Invitrogen), respectively. Cells were plated in 96-well culture plates at a density of 10000 cells per well (for the cytotoxicity) and 2000 cells per well (for the ROS measurement), and cultured overnight at 37 °C in a 5% CO_2 incubator. HeLa and NIH3T3 cells were cultured in Dulbecco's Modified Eagle Medium (DMEM, Gibco) supplemented with 10% fetal bovine serum, 1 mM L-glutamine, and 1% penicillin–streptomycin. HEL cells were cultured in Essential Minimum Eagle Medium with Earle's Salts (EMEM, Merk Millipore®) supplemented with 10% fetal bovine serum, 2 mM L-glutamine, non-essential amino acids (1x) (Merck Millipore®), sodium bicarbonate (0.2% w/v), and 2% penicillin–streptomycin. SKBR3 cells were cultured in McCoy's 5A Medium (Gibco) supplemented with 10% fetal bovine serum, and 1% penicillin–streptomycin.

For the cytotoxicity assay, cells were exposed to different amounts of enzyme (1–10 mU) and D-Ala concentrations (10–20 mM) for 24 h. After the removal of the growth medium, cells were washed with 100 μl 1x PBS pH 7.4 and incubated with 30 μl trypsin (0.25% w/v in ethylenediaminetetraacetic acid) for 10 min at 37 °C. After detachment, cells were incubated with 1 μl propidium iodite (1 mg ml^{-1}) and 2 μl of 50 μM calcein-AM in DMSO for 15 min at room temperature, in the dark. Fluorescent signal was measured using the flow cytometer BD FACSVerse™ Cell Analyzer (Bioscences) (red: ex. 495/em. 635 nm, green: ex. 495/em. 515 nm). Toxicity was quantified as the fraction of live cells relative to the total amount of counted cells. The analyses were replicated three times for each condition and the mean ± SD was calculated. Statistical analysis was performed comparing the viability of all the tested cell lines after their exposure to f-NDs (no DAAO) versus f-NDs-DAAO (no PC), and f-NDs (no DAAO) versus f-NDs-DAAO-PC. The statistical significance was determined at $p < 0.05$.

For the ROS measurement, cells were exposed to different amounts of enzyme (1–10 mU) and D-Ala concentrations (10–20 mM) and, immediately after the exposure, 2 μl of 0.5 mM oxidative stress indicator CM-H2DCFDA (Invitrogen) in DMSO was added to each well (10 μmol/L final concentration). The plates were incubated in the 5% CO_2 incubator for 40 min and the fluorescent signal was measured using the Infinite M200 PRO microplate reader (Tecan, Austria) with ex. 492/em. 527 nm. The measurement was repeated every 20 min for four hours (maximum time to avoid the degradation of the fluorescent probe), and then after 24 h (incubating cells with a new probe). The intensity of the signal was expressed relatively to the value obtained for controls (i.e., not treated cells). The analyses were replicated three times for each condition and the mean ± SD was calculated.

In both assays, the same protocol was applied to cells with and without the addition of f-NDs-DAAO-PC (i.e., HA-NDs-DAAO-PC, PEG-NDs-DAOO-PC and PGMA-NDs-DAAO-PC), to evaluate the effect of the PC on both the cytotoxicity and the induction of oxidative stress. Both assays were performed also on f-NDs (without DAAO) and on non-treated cells, as controls.

2.6. Fluorescent f-NDs-DAAO preparation and uptake analysis in cells

In order to make f-NDs-DAAO (i.e., HA-NDs-DAAO, PEG-NDs-DAAO and PGMA-NDs-DAAO) fluorescent, they were covalently functionalized with Alexa Fluor™ 750 NHS ester Tris(triethylammonium salt) (Invitrogen). In particular, a stock solution of f-NDs-DAAO was prepared suspending f-NDs-DAAO in 100 mM sodium pyrophosphate buffer pH 8.5 at final DAAO's concentration of 10 m g /m l . 0.1 ml of stock solution was incubated with 5 μl 10 mg/ml amine-reactive dye in anhydrous DMF (at 20:1 (v:v) ratio f-NDs-DAAO:dye) for 1 h at room temperature, under stirring. The fluorescent NDs were then collected by centrifugation (270 x g for 5 min at room temperature) and analyzed with a FLS 980 fluorescent spectrometer (Edinburgh Instruments) (ex. 753/em. 782 nm).

The uptake of fluorescent f-NDs-DAAO in HeLa, SKBR3, NIH3T3 and HEL cells was evaluated four hours after incubation with fluorescent f-NDs-DAAO. This time period was selected to compare the results with the ROS values (see paragraph 2.5). In particular, cells were plated in 96-well culture plates at a density of 10000 cells per well and cultured overnight at 37 °C in a 5% CO_2 incubator in their culture medium, as reported in paragraph 2.5. The medium was then exchanged for fresh medium with or without fluorescent f-NDs-DAAO (125 μg/mL) and the cells were incubated for 4 h. The medium was then removed, cells were washed with 100 μl 1x PBS pH 7.4 and incubated with 30 μl trypsin (0.25% in ethylenediaminetetraacetic acid) for 10 min at 37 °C, to detach them from the bottom of the wells. Then, 170 μl of fresh medium was added and the fluorescent signal

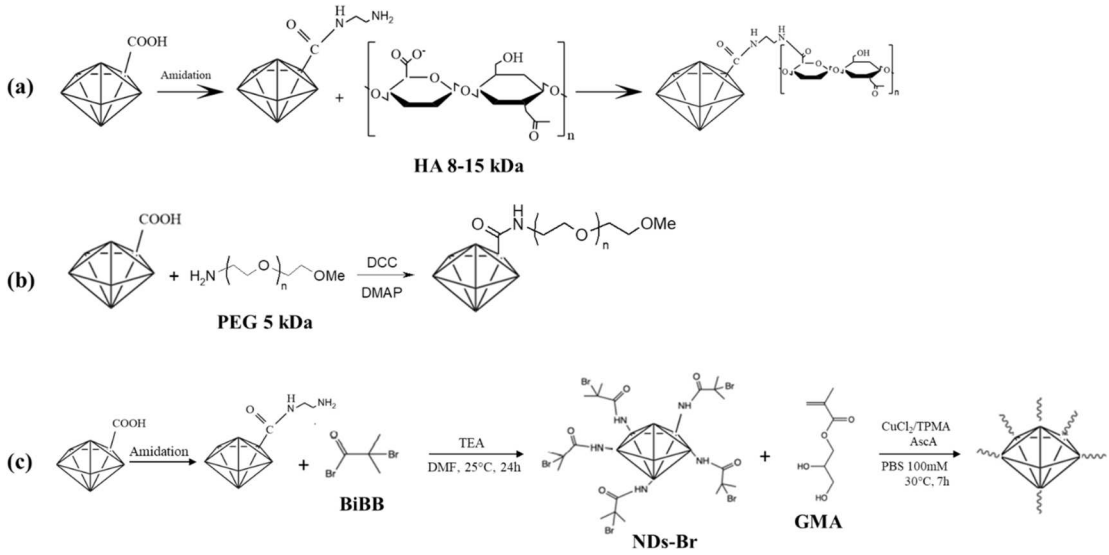

Figure 1. Scheme of NDs functionalization with (a) hyaluronic acid (HA), (b) polyethylene glycol (PEG) and (c) poly(glycerol monomethacrylate) (PGMA).

Table 1. Quantification of enzyme adsorbed on each NDs, and relative milligrams of functionalizing polymers covalently linked to the surface of NDs. Hydrodynamic size and z potential of HA-NDs-DAAO, PEG-NDs-DAAO and PGMA-NDs-DAAO, obtained with a DLS analysis performed in 1X PBS.

	HA-NDs-DAAO	PEG-NDs-DAAO	PGMA-NDs-DAAO
mg of polymer[a]	0.10	0.08	1.70
mg of DAAO[a]	1.65	1.52	0.55
Hydrodynamic size (nm)	241.0 ± 7.90	274.0 ± 1.40	610.0 ± 21.30
z potential (mV)	−8.66 ± 0.82	−11.80 ± 1.48	−3,89 ± 0.40

[a] on 2 mg of NDs

was recorded using the flow cytometer BD FACSVerse™ Cell Analyzer (Biosciences) (ex. 640/em. 783 nm). The analyses were replicated three times for each condition and the mean ± SD was calculated.

3. Results

3.1. Preparation and characterization of f-NDs-DAAO

COOH-NDs were functionalized with three different polymers, HA, PEG and PGMA, as reported in figure 1. All f-NDs were analyzed by TGA. As shown in figures S1 and S2(a), a functionalization degree (reported as percentage of loss of polymer mass, covalently linked on NDs' surface) of ~5% and ~4% for HA and PEG were obtained, respectively. A much higher functionalization degree (~85%) was obtained with PGMA, as a result of the more efficient grafting-from polymerization over the standard grafting-to approach [21, 22]. The functionalization with PGMA was also evaluated by the FTIR analysis, as shown in figure S2(b), where the spectra of COOH-NDs, PGMA-NDs and PGMA alone are compared. The characteristic peaks of PGMA (CH_2 and CH_3 groups stretching in the 2990–2880 cm^{-1} region, the double bond C=O stretching at 1714 cm^{-1} and C–O–C ester in the 1158–1049 cm^{-1} region) were observed for PGMA-NDs, highlighting the presence of the PGMA polymer on NDs' surface. The FTIR spectra of HA-NDs and PEG-NDs were not reported since the low functionalization degree does not generate visible peaks. From ^{1}H-NMR analysis, the PGMA obtained with the ARGET ATRP procedure had an average molecular mass of ~5 kDa.

Considering the enzyme's adsorption onto all f-NDs, after the incubation of 2 mg NDs with 3 mg DAAO, HA-NDs and PEG-NDs seemed to show similar enzyme's adsorption (~1.65 mg and ~1.52 mg, respectively), while PGMA-NDs showed a lower DAAO's adsorption (~0.55 mg) (table 1).

The hydrodynamic size of the f-NDs-DAAO in PBS was established by DLS measurements: 241.0 nm ± 7.9 nm for HA-NDs-DAAO, 274.0 nm ± 1.4 nm for PEG-NDs-DAAO, and 610.0 nm ± 21.3 nm for PGMA-NDs-DAAO. Moreover, a zeta potential of -8.66 ± 0.82 mV for HA-NDs-DAAO, -11.80 ± 1.48 mV for PEG-NDs-DAAO, and -3.89 mV ± 0.40 mV for PGMA-NDs-DAAO, was measured (table 1). Altogether, the

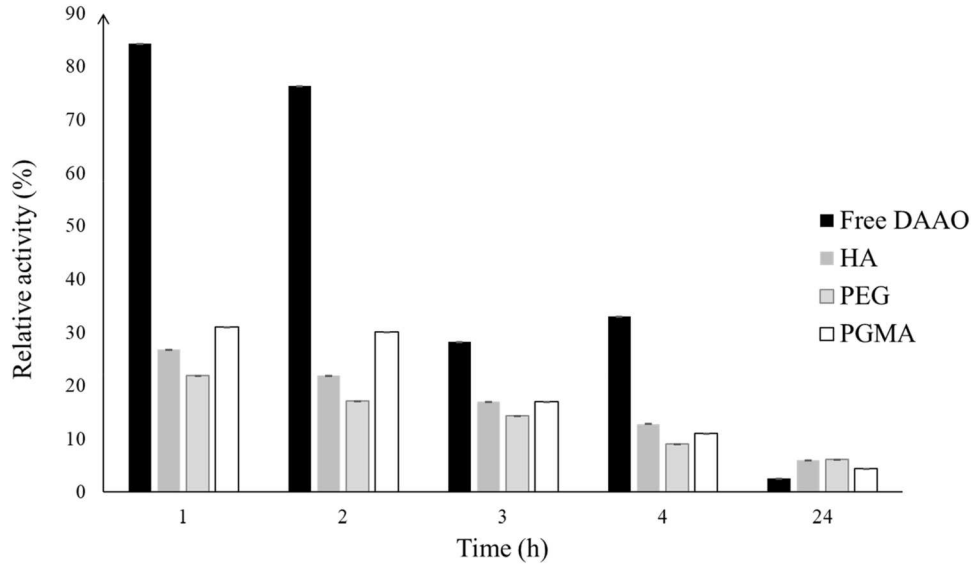

Figure 2. Enzyme stability at 37 °C. The assay was performed on free DAAO (black bars), COOH-NDs-DAAO (dark grey bars), HA-NDs-DAAO (grey bars), PEG-NDs-DAAO (light grey bars) and PGMA-NDs-DAAO (white bars). The activity value at 0 h for each sample is taken as 100%. The values are reported as mean ± standard deviation (n = 3).

functionalization with both HA and PEG seemed to contribute to reduce the nanoparticles' aggregation with respect to the functionalization with PGMA.

3.2. DAAO activity and stability

The enzymatic activity of HA-NDs-DAAO, PEG-NDs-DAAO and PGMA-NDs-DAAO was evaluated via a colorimetric assay. The apparent specific activity of DAAO linked to f-NDs was lower than the value for the free enzyme: a figure of 70, 56, 9 and 82 U/mg was apparent for HA-NDs-DAAO, PEG-NDs-DAAO, PGMA-NDs-DAAO and free DAAO, respectively.

Concerning the enzymatic stability, the free enzyme showed a linear decrease of activity up to 2 U/mg after 24 h incubation at 37 °C (i.e., 2.6% of the initial activity, not shown). For all f-NDs-DAAO samples, a similar trend was observed. Interestingly, the functionalization with both HA and PEG increased the stability of the enzyme at the longest time: a residual activity after 24 h of incubation at 37 °C of ~6% of the initial figure was measured (figure 2). f-NDs alone (without DAAO) showed no activity.

3.3. Protein corona investigation

To investigate the PC formation around f-NDs-DAAO, an *in vitro* incubation in HS was performed, and proteins belonging to SC and HC were collected. An elution protocol based on sequential steps using solutions at different ionic strength and temperature, was applied. SC proteins were eluted by native buffers (i.e., E1 and E2) at 37 °C, while HC proteins were eluted by a denaturant buffer, E3, at 99 °C. The formation of the PC depended on the type of functionalization on NDs' surface. HA-NDs-DAAO and PEG-NDs-DAAO showed less intense SDS-PAGE profiles (figure S3(a)) due to a less concentrated SC (figure S3(b)) (i.e., ~1 mg ml^{-1}) with respect to PGMA-NDs-DAAO (~2 mg ml^{-1}). Mass spectrometry analysis identification of the SC proteins demonstrated that PEG-NDs-DAAO showed a reduced heterogeneity of the PC: a total of 32, 42 and 52 proteins were identified in the SC (figure 3(a)), and 4, 8 and 6 identified proteins in the HC (figure 3(b)) in PEG-NDs-DAAO, HA-NDs-DAAO and PGMA-NDs-DAAO, respectively. PEG-NDs-DAAO improved the interaction with immune system's inhibitors in the SC (from figure 3(a), 25% versus 21% versus 19% for PEG-NDs-DAAO, PGMA-NDs-DAAO and HA-NDs-DAAO, respectively), and it was the only one not containing immune system's activators in the HC (figure 3(b)).

3.4. *In vitro* cytotoxicity assay and ROS level measurement

The cytotoxicity and the oxidative stress induced by f-NDs, f-NDs-DAAO and f-NDs-DAAO-PC on human tumor (HeLa and SKBR3) and human and murine healthy (HEL and NIH3T3) cell lines were investigated, using D-Ala as the optimal substrate. The cytotoxicity was determined by the LIVE/DEAD cytotoxicity/viability test, after the exposure of cells to NDs for 24 h. The induction of oxidative stress, mainly due to the production of H_2O_2, was determined 40 min after the exposure of cells to NDs, then every 20 min for 4 h and at 24 h, using the oxidative stress indicator CM-H2DCFDA [30]. The assay revealed that f-NDs alone (i.e., not

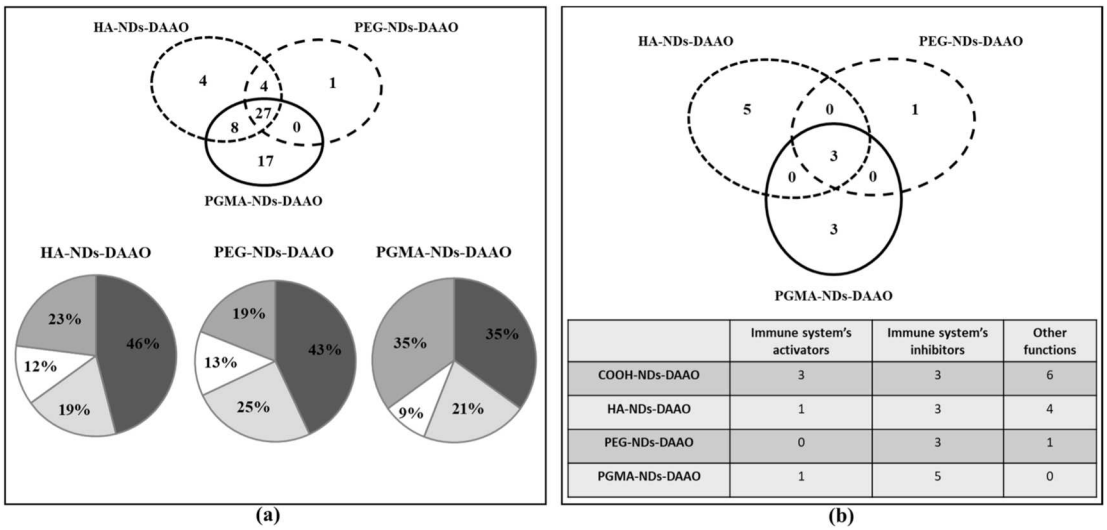

	Immune system's activators	Immune system's inhibitors	Other functions
COOH-NDs-DAAO	3	3	6
HA-NDs-DAAO	1	3	4
PEG-NDs-DAAO	0	3	1
PGMA-NDs-DAAO	1	5	0

Figure 3. Venn diagrams and Pie Charts to compare (a) the soft corona and (b) the hard corona protein composition of HA-NDs-DAAO, PEG-NDs-DAAO and PGMA-NDs-DAAO. In all Pie Charts, the dark grey sector contained proteins able to activate immune response, the light grey one reported proteins devoted to inhibit the defensive processes, the white one referred to proteins favoring the cells adhesion and the grey one was characterized by proteins with different functions.

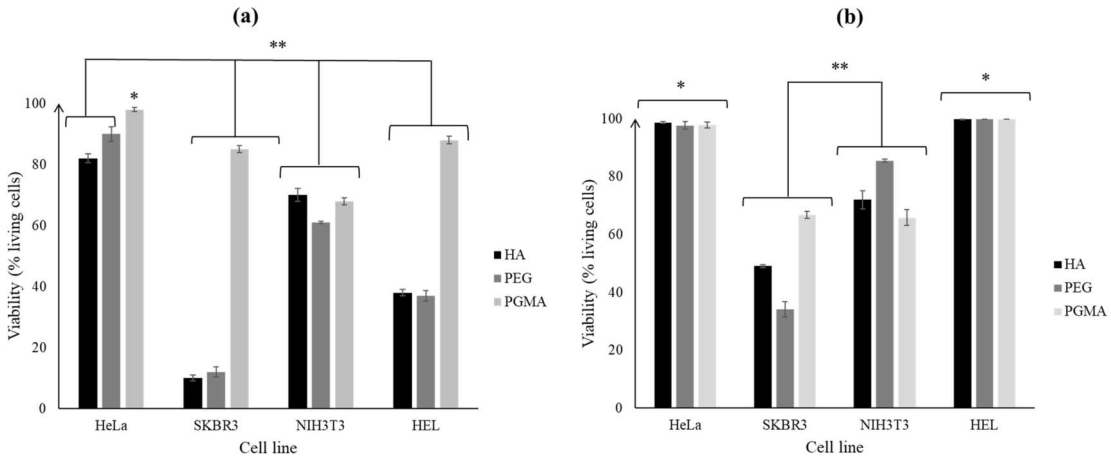

Figure 4. Cytotoxicity induced by (a) HA-NDs-DAAO-PC (black bars), PEG-NDs-DAAO-PC (dark grey bars) or PGMA-NDs-DAAO-PC (light grey bars), and by (b) HA-NDs-DAAO (black bars), PEG-NDs-DAAO (dark grey bars) and PGMA-NDs-DAAO (light grey bars) on HeLa and SKBR3 tumor cell lines and NIH3T3 and HEL healthy cell lines. The cytotoxicity was assessed with the LIVE/DEAD cytotoxicity/viability test, after 24 h of cells' incubation with 10 mU enzyme and 20 mM D-Ala as substrate. The results are expressed as the percentage of living cells on the total amount of counted cells and the values are reported as mean ± standard deviation (n = 3). Data were analysed for statistical significance, comparing the viability of all the tested cell lines treated with (a) f-NDs (without DAAO) versus f-NDs-DAAO-PC, and (b) f-NDs (without DAAO) versus f-NDs-DAAO (no PC). $^{*}p > 0.05$ and not statistically significant, $^{**}p < 0.01$.

conjugated with DAAO) did not induce cytotoxicity in either tumor or healthy cells (figure S4(a)) and did not produce ROS (the fluorescence intensity almost constant and equal to untreated cells, figure S4(b)).

The concentration of both the enzyme and D-Ala, used for the experiments, seemed to influence cytotoxicity and oxidative stress. As shown in figure S5(a), SKBR3 cells treated with 10 mU DAAO showed lower viability than cells treated with 1 mU DAAO. Concerning the ROS measurement, the fluorescent signals during the treatment at the highest amount of DAAO (i.e., 10 mU) were at least 4-fold higher than the ones at 1 mU of enzyme (figure S5(b)). Similar results were observed as a function of D-Ala concentration: its increase led to a higher f-NDs-DAAO cytotoxicity, as a consequence of a higher oxidative stress (not shown).

For all the tested human cell lines, the treatment with HA-NDs-DAAO-PC or PEG-NDs-DAAO-PC (figure 4(a)) enhanced the cytotoxic effect compared to the f-NDs-DAAO counterpart (figure 4(b)). SKBR3 cells, showing the lowest viability, the presence of PC led to a mortality rate of ~90% (with respect to a maximum of 66% reached with HA-NDs-DAAO). HeLa cells showed a negligible mortality, slightly higher when

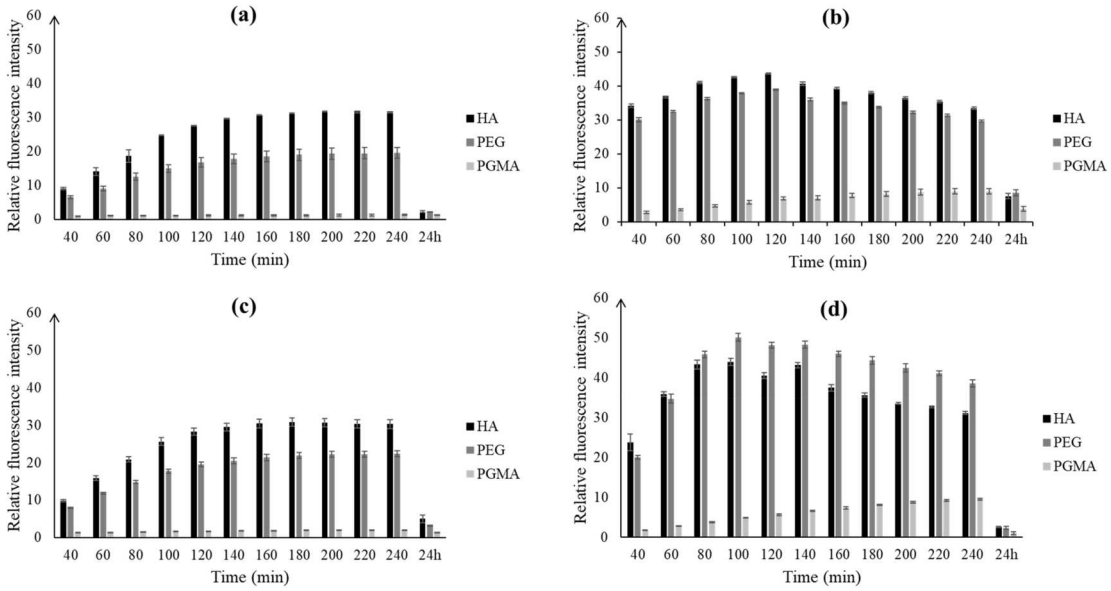

Figure 5. ROS levels after the treatment with HA-NDs-DAAO-PC (black bars), PEG-NDs-DAAO-PC (dark grey bars) or PGMA-NDs-DAAO-PC (light grey bars) of (a) HeLa, (b) SKBR3, (c) NIH3T3 and (d) HEL cells. Cells were exposed to 10 mU enzyme and 20 mM D-Alanine. The intensity of the signal is expressed as a function of the intensity of controls (i.e., not treated cells, set as 1). The values are reported as mean ± standard deviation (n = 3).

threated with HA-NDs-DAAO-PC (~20%) and PEG-NDs-DAAO-PC (~10%) (figure 4(a)). HEL 12469 healthy human cells were not affected by f-NDs-DAAO (viability ~100%), and appeared more susceptible to HA-NDs-DAAO-PC and PEG-NDs-DAAO-PC (viability ~38%). On the contrary, the presence of the PC on NDs' surface did not enhance the mortality of NIH3T3 healthy murine cells, characterized by a ~70% viability after the treatment with f-NDs-DAAO or f-NDs-DAAO-PC.

For all the tested cell lines, the PC enhanced the intensity of the ROS fluorescent signals, especially when cells were treated with HA-NDs-DAAO-PC and PEG-NDs-DAAO-PC (figure 5 and figure S6, respectively). In particular, the significantly higher levels of ROS recorded in SKBR3 and HEL already after 40 min of treatment with HA-NDs-DAAO-PC (34 and 24 for SKBR3 and HEL, respectively) and PEG-NDs-DAAO-PC (30 and 20 for SKBR3 and HEL, respectively) with respect to HeLa (9 with HA-NDs-DAAO-PC and 6 with PEG-NDs-DAAO-PC) and NIH3T3 (10 with HA-NDs-DAAO-PC and 8 with PEG-NDs-DAAO-PC), reflected the higher cytotoxic effect observed in SKBR3 and HEL cells.

The treatment with PGMA-NDs-DAAO or PGMA-NDs-DAAO-PC appeared less effective in inducing the cell death (maximum of 35%). Moreover, the ROS levels were significantly lower. In all cell lines, the ROS level at 24 h after exposure to f-NDs-DAAO or f-NDs-DAAO-PC was very low, corresponding to the near-total loss of DAAO activity after 24 h, with a consequent drop in hydrogen peroxide production.

3.5. Uptake of fluorescent f-NDs-DAAO

The successful labelling of f-NDs-DAAO with the fluorescent amine-reactive dye was confirmed by the spectrophotometric analysis, as shown in figure S7 by exciting the f-NDs at 753 nm: a peak at around 782 nm was recorded, confirming the presence of the dye on NDs surface.

The uptake of f-NDs-DAAO into HeLa, SKBR3, NIH3T3 and HEL cells was evaluated after four hours of exposure of cells to 125 μg/mL f-NDs-DAAO using flow cytometry. In all tested cell lines, HA-NDs-DAAO underwent the highest uptake, followed by PEG-NDs-DAAO and, lastly, by PGMA-NDs-DAAO (figure 6). Both HA-NDs-DAAO and PEG-NDs-DAAO were internalized more by HeLa and NIH3T3 cells, while the uptake by SKBR3 and HEL cells was limited. PGMA-NDs-DAAO showed the highest internalization in NIH3T3. Overall, NIH3T3 cell lines showed the highest uptake of all f-NDs-DAAO, while the lowest uptake was apparent for SKBR3 cells.

4. Discussion

To properly design a promising nanocarrier for therapeutic anticancer enzyme, a well-characterized and promising enzyme for EPT applications was selected, called DAAO, and NDs were functionalized to improve their biocompatibility. In detail, three polymers, namely HA, PEG and PGMA (figure 1), were chosen for their

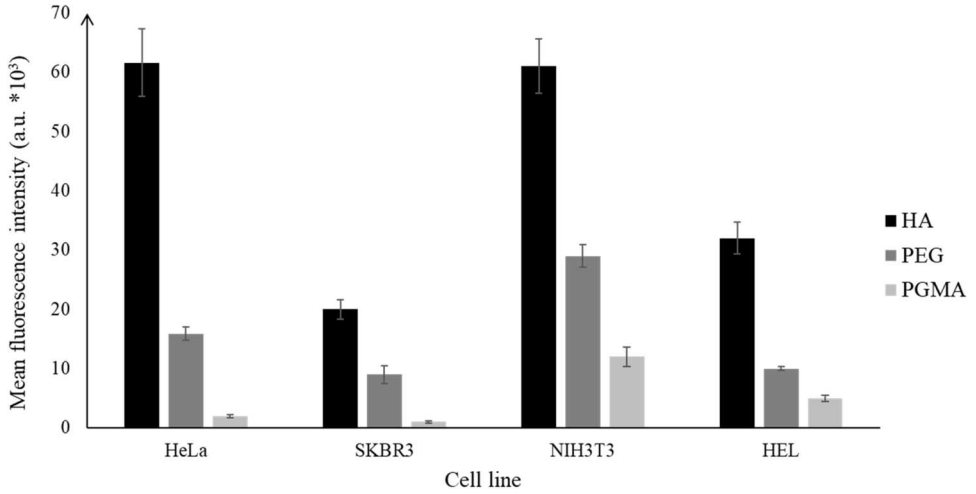

Figure 6. Uptake of HA-NDs-DAAO (black bars), PEG-NDs-DAAO (dark grey bars) or PGMA-NDs-DAAO (light grey bars) in HeLa and SKBR3 cancer cells, and NIH3T3 and HEL healthy cells. The fluorescence was measured after cells' exposure to 125 μg NDs/mL for a total of four hours. The values are reported as mean ± standard deviation (n = 3).

well-documented suitability in biomedical applications, including increased blood circulation time, stealth properties and reduced NPs' aggregation [9, 21, 31].

All the three tested polymers were characterized by a comparable molecular mass (5 kDa for PEG, 8–15 for kDa HA and 5 kDa for PGMA): particularly, 5 kDa PEG was chosen because widely used to prepare polymeric drugs and of its capability of preserving the DAAO's cytotoxic effect [18, 32]. NDs reached a functionalization level of 5% for HA, 4% for PEG and 85% for PGMA, as shown in figures S1 and S2(a). The high functionalization degree obtained with PGMA allows to maximize the interaction between PGMA and NDs. The modification of NDs surface with PGMA was also confirmed by the FTIR spectra (figure S2(b)), where PGMA-NDs and PGMA alone shared the same characteristic peaks.

The NDs coupling with the DAAO, a well-characterized flavoenzyme in terms of kinetics and turnover, was aimed to regulate the ROS production via a controlled D-amino acid administration, thus preventing damages to normal tissues and allowing the so called 'activity on demand' directly into tumor site, mitigating the side effects of current anticancer therapy [1]. The functionalization degree on the NDs' surface seemed to play a crucial role in the interaction with DAAO: the increase of functionalization degree and of polymers' steric hindrance, as a consequence, could limit the enzyme adsorption (table 1). HA-NDs and PEG-NDs, with a similar functionalization degree (~4–5), showed a similar DAAO binding level (~ 1.65 mg and ~1.5 mg of DAAO, respectively), while PGMA-NDs, with the highest functionalization degree (~85%), adsorbed the lowest amount of enzyme (~ 0.55 mg). The correlation between functionalization and enzymatic adsorption was already observed in our previous work, where the presence of PEG molecules on carbon nanotubes' surface led to a reduction of DAAO's adsorption, with respect to carboxylated nanotubes [33]. Dynamic light scattering (DLS) analysis was performed to characterize the hydrodynamic size and zeta potential of the formulated f-NDs-DAAO in suspension. Given their potential for intravenous administration, assessment of colloidal stability was prioritized over morphological characterization of individual particles by high-resolution transmission electron microscopy (HR-TEM). DLS measurements indicated that the functionalization with HA and PEG reduced the aggregation of f-NDs-DAAO, and yielded a hydrodynamic size of ~240–270 nm. In physiological-like media, their colloidal stability was also confirmed by the zeta potential measurement: the lower values were determined for HA-NDs-DAAO and PEG-NDs-DAAO (-8.7 mV and -11.8 mV, respectively) with respect to PGMA-NDs-DAAO (-7.94 mV and -3.9 mV, respectively), as reported in table 1.

The activity and stability of f-NDs-DAAO conjugates were evaluated, confirming the already well-established data reported in literature such as the time-dependent decrease of DAAO's activity at 37 °C and the lower activity of the enzyme adsorbed on NDs' surface in comparison with the free form [6]. Interestingly, the functionalization with HA and PEG favoured the long-time stability of the enzyme after 24 h, supporting the positive effect of both PEG and HA conjugation (figure 2) [18].

The biocompatibility of f-NDs-DAAO was evaluated incubating the nanosystems in HS and investigating the composition of the PC formed on NDs' surface, as bio-corona formation has been shown to significantly affect the biological fate of nanostructures. In fact, the PC could favor the circulation of NPs in the blood stream, preventing the clearance by the immune system, and enhance the targeting to the tumor site [13, 34]. Moreover, the PC could alter the interaction of NPs with cells, favoring the NPs' adhesion and therefore the

therapeutic effect [35, 36]. The PC composition was evaluated, distinguishing between HC and SC. The HC is quickly formed after the incubation of NPs with biological fluids, and it is more stable in composition, containing proteins with high affinity to the NPs' surface. The SC takes more time to reach the equilibrium, and it is a more exchangeable layer, composed by proteins that do not interact directly with the nanostructure, but with the proteins of the HC [37]. Physicochemical properties of NPs (e.g., surface chemistry and morphology) influence the adsorption of human proteins, determining the characteristics of the PC [15]. In fact, from the obtained results, the different functionalizations significantly influenced the formation of both SC and HC. PEG-NDs-DAAO was characterized by a less variegate PC. The amount of SC, very similar the one of HA-NDs-DAAO (~1 mg ml^{-1}), was significantly lower than the SC of PGMA-NDs-DAAO (~2 mg ml^{-1}) (figure S3(b)), reflecting less intense protein profiles in SDS-PAGE gel (figure S3(a)). The mass spectrometry analysis showed that the number of different proteins, and therefore the variegation, was reduced in PEG-NDs-DAAO: the numbers of identified proteins were 32, 42 and 52 in the SC (figure 3(a)), and 4, 8 and 6 in the HC (figure 3(b)) in PEG-NDs-DAAO, HA-NDs-DAAO and PGMA-NDs-DAAO, respectively.

Considering the identified biomolecules and the biological processes in which they are involved, the SC of all f-NDs-DAAO was characterized by similar profiles (figure 3(a)). Opsonins, like Igs and complement's system components (i.e., complement C3) were identified, as well as Apos and immune system's inhibitors (i.e., albumin and plasma protease C1 inhibitor). As reported in literature, albumin can reduce both the adsorption of plasma proteins and the complement activation, prolonging the NPs' circulation in blood [38]. Plasma protease C1 inhibitor forms a proteolytically inactive complex with the C1r or C1s proteases, downregulating the complement system [39]. Interestingly, proteins involved in cell membrane adhesion were also identified. Inter-alpha-trypsin inhibitor heavy chain H2 binds hyaluronan on the cells' surface and this suggested the possible tendency of HA-NDs to interact with cells [40]. Interesting, as stated in literature, serotransferrin is one of the most investigated ligands for NPs' functionalization, since several tumor cell membranes (like the blood–brain barrier) and tumor cells (e.g., SKBR3), overexpress transferrin receptors on their surface [41–43]. The possibility to enrich the SC in these proteins could be crucial to potentially promote NPs interactions with human tissues, thus enhancing the NPs' association with human tumor cells. Surprisingly, antioxidants were identified only in the SC of PGMA-NDs-DAAO. Glutathione peroxidase 3 and protein AMBP (whose cleavage forms Alpha-1 microglobulin) protects cells from oxidative damages, by catalyzing the reduction of H_2O_2 [44–48]. These proteins could neutralize the H_2O_2 produced by DAAO, probably reducing the therapeutic effect.

The HC was mostly characterized by immune system's inhibitors, like histidine-rich glycoprotein, Apos like Apo A-1, and albumin. In comparison to HA-NDs-DAAO and PGMA-NDs-DAAO, that interacted specifically with Ig kappa constant and Ig lambda constant 6, respectively, no immune system's activators or Igs were identified in HC of PEG-NDs-DAAO. Further, the HC of PEG-NDs-DAAO exclusively contained Apo A-1 and Histidine-rich glycoprotein, an Igs inhibitor: it binds IgG subclasses containing kappa and lambda light chains, inhibiting the formation of insoluble immune complexes (figure 3(b)) [49–51].

The cytotoxicity of f-NDs-DAAO, f-NDs-DAAO-PC and f-NDs on cancer (i.e., HeLa and SKBR3) and healthy (i.e., NIH3T3 and HEL) cell lines. As expected, no cytotoxic effect was observed after administration of f-NDs (figure S4(a)): their inability of producing significant H_2O_2 amount was confirmed by the ROS levels measurement test (figure S4(b)) [52]. Therefore, considering that DAAO was essential for the cytotoxicity and for designing a therapeutically effective nanosystem, using higher DAAO (figure S5(a)) and D-Ala concentrations (data not shown) resulted into a higher cytotoxicity (i.e., lower viability). These results were also confirmed by ROS measurements: cells treated with 10 mU of enzyme and 20 mM of D-Ala increased the induction of oxidative stress (figure S5(b)).

The bio-corona seemed to enhance the H_2O_2 production and the cytotoxicity induced by f-NDs-DAAO on the different selected human cell lines. One hypothesis, also described in literature, could be that the presence in the bio-corona of proteins like Serotransferrin and inter-alpha-trypsin inhibitor heavy chain H2, may contribute to favor the interaction between NPs and human cells' surface receptors, enhancing both the oxidative stress (the signals reported in figure 5 after the treatment with f-NDs-DAAO-PC reached higher intensities than the signals in figure S6 for f-NDs-DAAO) and the cytotoxicity (figure 4(a) about f-NDs-DAAO-PC versus figure 4(b) about f-NDs-DAAO) [40, 41]. For this reason, PC particularly seemed to enhance the *in vitro* cytotoxicity against the cancerous cell line SKBR3, characterized by the highest mortality especially after the treatment with PEG-NDs-DAAO-PC: the cytotoxicity on human breast carcinoma cells increased by 75% after the incubation for 24 h with 10 mU of PEG-NDs-DAAO-PC (figure 4(a)), in comparison with the PEG-NDs-DAAO counterpart (figure 4(b)). The enhancement in oxidative stress, probably also favored by PC composition (figure 5(b) and figure S6(b)), and the lower expression of antioxidative enzymes, peculiar of human cancer cells (more susceptible to the ROS treatment than healthy cells), could probably play an important role in SKBR3 cell's death [53]. On the contrary, HEL and NIH3T3 healthy cell lines showed a higher resistance against the treatment with DAAO compared to cancerous breast carcinoma (i.e., SKBR3 cells), confirming their basal

expression of antioxidative enzymes [54, 55]. On this side, human fibroblast appeared more susceptible to the treatment than mouse fibroblast (figure 4(a)), possibly due to a higher interaction of f-NDs-DAAO-PC with HEL cells [40, 42, 43, 56, 57]. Even if the PC slightly reduced the viability of immortalized cervical cancer cell line (i.e., HeLa) (~100% versus ~80% with HA-NDs-DAAO and HA-NDs-DAAO-PC, respectively), the treatment appeared ineffective, confirming, as reported in literature, that HeLa cells are characterized by a multi drug resistance [58]. Moreover, the higher level of antioxidative enzymes, normally present in HeLa cells, could potentially inactivate the H_2O_2 produced by DAAO [59, 60].

Among all tested f-NDs-DAAO-PC, the lowest cytotoxic effect was observed for PGMA-NDs-DAAO-PC: the lower stability of DAAO adsorbed on PGMA-NDs (figure 2) and the presence in the corresponding PC of antioxidative enzymes (i.e., glutathione peroxidase 3 and protein AMBP) could probably contribute to hamper the cytotoxic effect [44–48]. Actually, the fluorescence signals associated with ROS production by PGMA-NDs-DAAO-PC appeared significantly lower than the signals measured with the other nanostructures (figure 5, light gray bars), suggesting a lower oxidative stress. Considering all the obtained results, the excessive size (610.0 nm $\pm$ 21.3 nm), the composition of the PC and the limited cytotoxicity, on the tested tumor cell lines, led to hypothesize that PGMA-NDs-DAAO would not suitable for therapeutic applications [61].

Finally, comparing the ROS signals at 240 min with the results of uptake, no direct correlation between the induction of oxidative stress and the nanoparticles' uptake in cells was apparent (figures S6 and figure 6). The bystander effect of extracellular H_2O_2 (produced by not yet internalized NDs) inside cells seemed to be the most predominant mechanism for the oxidative stress. Recent studies identified H_2O_2 as a new substrate for several members of aquaporins [62, 63]. This bystander effect could suggest that the NPs' uptake inside cells could be not necessary for killing adjacent tumor cells, making the cytotoxic effect easier to be achieved.

5. Conclusion

In the present study, carboxylated NDs were functionalized with three different biocompatible polymers (i.e., HA, PEG and PGMA), and the well-characterized DAAO flavoenzyme was adsorbed on their surface to design promising therapeutic nanosystems for antitumor therapy. Their bio-interface was investigated, evaluating their interaction with human serum, and the role of the PC on their *in vitro* cytotoxicity was elucidated. The functionalization with PEG seemed to play a synergistic role in the generation of oxidative stress and the formation of bio-corona. PEG-NDs-DAAO protein-corona was enriched in dysopsonins (particularly Apo 1-A) and low in immune system's activators, thus leading the hypothesis of a prolonged blood circulation time and a reduced clearance. Interestingly, the identification in the PC of proteins involved in tumor cell adhesion could play an important role in the target of human breast carcinoma, generating a significant cytotoxic effect.

Acknowledgments

We acknowledge the Research Infrastructure NanoEnviCz, supported by the Ministry of Education, Youth and Sports of the Czech Republic under Project No. LM2023066. The work was supported from European Regional Development Fund—Project Excellence in Regenerative Medicine' (No. CZ.02.01.01/00/22_008/0004562). ER and LP thank the support from Fondo di Ateneo per la Ricerca and the CIB project 2024 'Nuove tendenze per le applicazioni biotecnologiche'.

Conflict of interest

The authors have declared no conflict of interest.

Data availability statement

All data that support the findings of this study are included within the article (and any supplementary files).

References

[1] Rosini E and Pollegioni L 2022 Reactive oxygen species as a double-edged sword: the role of oxidative enzymes in antitumor therapy *BioFactors* **48** 384–99

[2] Pollegioni L, Molla G, Sacchi S, Rosini E, Verga R and Pilone M S 2008 Properties and applications of microbial D-amino acid oxidases: current state and perspectives *Appl. Microbiol. Biotechnol.* **78** 1–16

[3] Ibañez I L, Notcovich C, Catalano P N, Bellino M G and Durán H 2015 The redox-active nanomaterial toolbox for cancer therapy *Cancer Lett* **359** 9–19

[4] Pollegioni L, Kustrimovic N, Piubelli L, Rosini E, Rabattoni V and Sacchi S 2025 d-amino acids: new functional insights *FEBS J.* **292** 4395–417
[5] Marcone G L, Rosini E, Crespi E and Pollegioni L 2019 D-amino acids in foods *Appl. Microbiol. Biotechnol.* **104** 555–74
[6] Boreggio M, Rosini E, Gambarotti C, Pollegioni L and Fasoli E 2022 Unveiling the Bio-corona fingerprinting of potential anticancer carbon nanotubes coupled with d-amino acid oxidase *Mol. Biotechnol.* **64** 1164–76
[7] Bava A, Gornati R, Cappellini F, Caldinelli L, Pollegioni L and Bernardini G 2013 D-amino acid oxidase-nanoparticle system: a potential novel approach for cancer enzymatic therapy *Nanomedicine* **8** 1797–806
[8] Tjo K and Varamini P 2022 Nanodiamonds and their potential applications in breast cancer therapy: a narrative review *Drug Deliv. Transl. Res.* **12** 1017–28
[9] Leung H M, Chu H C, Mao Z W and Lo P K 2023 Versatile nanodiamond-based tools for therapeutics and bioimaging *Chem. Commun.* **59** 2039–55
[10] Wu J, Du X, Zhang D, Cui J, Zhang X, Duan X, Trant J F and Li Y 2023 A nanodiamond chemotherapeutic folate receptor-targeting prodrug with triggerable drug release *Int. J. Pharm.* **630** 122432
[11] Hajipour M J *et al* 2023 An overview of nanoparticle protein corona literature *Small* **19** e2301838
[12] Lee H 2023 Differences in protein distribution, conformation, and dynamics in hard and soft coronas: dependence on protein and particle electrostatics *Phys. Chem. Chem. Phys.* **7496** 7496
[13] Kopac T 2021 Protein corona, understanding the nanoparticle-protein interactions and future perspectives: a critical review *International Journal of Biological Macromolecule* **169** 290–301
[14] Panico S, Capolla S, Bozzer S, Toffoli G, Dal Bo M and Macor P 2022 Biological features of nanoparticles: protein corona formation and interaction with the immune system *Pharmaceutics* **14** 2605
[15] Bilardo R, Traldi F, Vdovchenko A and Resmini M 2022 Influence of surface chemistry and morphology of nanoparticles on protein corona formation *Wiley Interdiscip. Rev. Nanomed. Nanobiotechnol.* **14** e1788
[16] Fuentes-Cervantes A, Ruiz Allica J, Calderón Celis F, Costa-Fernández J M and Ruiz Encinar J 2023 The potential of ICP-MS as a complementary tool in nanoparticle–protein corona analysis *Nanomaterials* **13** 1132
[17] Shilpi S, Gulbake A S, Chouhan S and Kumar P 2023 Functionalized carbon nanotubes, graphene oxide, fullerenes, and nanodiamonds: emerging theranostic nanomedicines *Multifunctional And Targeted Theranostic Nanomedicines* (Springer Nature Singapore) 187–213
[18] Rosini E and Pollegioni L 2020 PEG-DAAO conjugate: A promising tool for cancer therapy optimized by protein engineering *Nanomedicine* **24** 102122
[19] Alsaikhan F 2023 Hyaluronic acid-empowered nanotheranostics in breast and lung cancers therapy *Environ. Res.* **237** 116951
[20] Robert-Nicoud G, Evans R, Vo C D, Cadman C J and Tirelli N 2013 Synthesis, self-assembly and (absence of) protein interactions of poly(glycerol methacrylate)–silicone macro-amphiphiles *Polym. Chem.* **4** 3458–70
[21] Moncalvo F, Lacroce E, Franzoni G, Altomare A, Fasoli E, Aldini G, Sacchetti A and Cellesi F 2022 Protein-friendly atom transfer radical polymerisation of glycerol(monomethacrylate) in buffer solution for the synthesis of a new class of polymer bioconjugates *React. Funct. Polym.* **175** 105264
[22] Moncalvo F, Lacroce E, Franzoni G, Altomare A, Fasoli E, Aldini G, Sacchetti A and Cellesi F 2022 Selective Protein Conjugation of Poly(glycerol monomethacrylate) and Poly(polyethylene glycol methacrylate) with Tunable Topology via Reductive Amination with Multifunctional ATRP Initiators for Activity Preservation *Macromolecules* **55** 7454–68
[23] Pollegioni L and Molla G 2011 New biotech applications from evolved D-amino acid oxidases *Trends Biotechnol.* **29** 276–83
[24] Khan S *et al* 2022 Artificial engineering of the protein corona at bio-nano interfaces for improved cancer-targeted nanotherapy *J. Controlled Release* **348** 127–47
[25] Li H, Wang Y, Tang Q, Yin D, Tang C, He E, Zou L and Peng Q 2021 The protein corona and its effects on nanoparticle-based drug delivery systems *Acta Biomater.* **129** 57–72
[26] Fantinato S, Loredano P and Mirella P S 2001 Engineering, expression and purification of a His-tagged chimeric D-amino acid oxidase from Rhodotorula gracilis *Enzyme Microb. Technol.* **29** 407–12
[27] Molla G, Porrini D, Job V, Motteran L, Vegezzi C, Campaner S, Pilone M S and Pollegioni L 2000 Role of arginine 285 in the active site of rhodotorula gracilis d-amino acid oxidase: a site-directed mutagenesis study * *J. Biol. Chem.* **275** 24715–21
[28] Rosini E, Caldinelli L and Piubelli L 2017 Assays of D-amino acid oxidase activity *Front. Mol. Biosci.* **4** 102
[29] Nicoletti M, Gambarotti C and Fasoli E 2021 Proteomic exploration of soft and hard biocorona onto PEGylated multiwalled carbon nanotubes *Biotechnol. Appl. Biochem.* **68** 1003–13
[30] Jakubowski W and Bartosz G 2000 2,7-dichlorofluorescin oxidation and reactive oxygen species: what does it measure? *Cell Biol. Int.* **24** 757–60
[31] Yasin A, Ren Y, Li J, Sheng Y, Cao C and Zhang K 2022 Advances in hyaluronic acid for biomedical applications *Front. Bioeng. Biotechnol.* **10** 910290
[32] Gref R, Lück M, Quellec P, Marchand M, Dellacherie E, Harnisch S, Blunk T and Müller R H 2000 Stealth' corona-core nanoparticles surface modified by polyethylene glycol (PEG): influences of the corona (PEG chain length and surface density) and of the core composition on phagocytic uptake and plasma protein adsorption *Colloids Surf. B Biointerfaces* **18** 301–13
[33] Rosini E, Boreggio M, Verga M, Caldinelli L, Pollegioni L and Fasoli E 2023 The D-amino acid oxidase-carbon nanotubes: evaluation of cytotoxicity and biocompatibility of a potential anticancer nanosystem *3 Biotech* **13** 1–11
[34] Wang X and Zhang W 2022 The Janus of Protein Corona on nanoparticles for tumor targeting, immunotherapy and diagnosis *J. Controlled Release* **354** 832–50
[35] Kopac T 2021 Protein corona, understanding the nanoparticle–protein interactions and future perspectives: A critical review *Int. J. Biol. Macromol.* **169** 290–301
[36] Liu N, Tang M and Ding J 2020 The interaction between nanoparticles-protein corona complex and cells and its toxic effect on cells *Chemosphere* **245** 125624
[37] García-Álvarez R and Vallet-Regí M 2021 Hard and soft protein corona of nanomaterials: analysis and relevance *Nanomaterials* **11** 888
[38] Peng Q, Zhang S, Yang Q, Zhang T, Wei X-Q, Jiang L, Zhang C-L, Chen Q-M, Zhang Z-R and Lin Y-F 2013 Preformed albumin corona, a protective coating for nanoparticles based drug delivery system *Biomaterials* **34** 8521–30
[39] de Boer E C W *et al* 2023 C1-inhibitor treatment in patients with severe complement-mediated autoimmune hemolytic anemia *Blood Adv.* **7** 3128–39
[40] Kobos L and Shannahan J 2020 Biocorona-induced modifications in engineered nanomaterial–cellular interactions impacting biomedical applications *WIREs Nanomedicine and Nanobiotechnology* **12** e1608

[41] Abuzaid H, Abdelrazig S, Ferreira L, Collins H M, Kim D H, Lim K H, Kam T S, Turyanska L and Bradshaw T D 2022 Apoferritin-encapsulated jerantinine a for transferrin receptor targeting and enhanced selectivity in breast cancer therapy *ACS Omega* **7** 21473–82
[42] Sepand M R *et al* 2020 Impact of plasma concentration of transferrin on targeting capacity of nanoparticles *Nanoscale* **12** 4935–44
[43] Choudhury H *et al* 2018 Transferrin receptors-targeting nanocarriers for efficient targeted delivery and transcytosis of drugs into the brain tumors: a review of recent advancements and emerging trends *Drug Deliv. Transl. Res.* **8** 1545–63
[44] Ungati H, Govindaraj V, Narayanan M and Mugesh G 2019 Probing the formation of a seleninic acid in living cells by the fluorescence switching of a glutathione peroxidase mimetic *Angew. Chem.* **131** 8240–4
[45] Abdel-Daim M M, Abo El-Ela F I, Alshahrani F K, Bin-Jumah M, Al-Zharani M, Almutairi B, Alyousif M S, Bungau S, Aleya L and Alkahtani S 2020 Protective effects of thymoquinone against acrylamide-induced liver, kidney and brain oxidative damage in rats *Environmental Science and Pollution Research* **27** 37709–17
[46] Rezayian M, Niknam V and Ebrahimzadeh H 2019 Oxidative damage and antioxidative system in algae *Toxicol. Rep.* **6** 1309–13
[47] Weiss R, Meersch M, Wempe C, von Groote T, Agervald T and Zarbock A 2023 Recombinant alpha-1-microglobulin (RMC-035) to prevent acute kidney injury in cardiac surgery patients: phase 1b evaluation of safety and pharmacokinetics *Kidney Int Rep* **8** 980–8
[48] Lopez D 2020 Identification of novel proteins interacting with proprotein convertase subtilisin/kexin 9 *Int. J. Biomed. Investig.* **3** 1–17
[49] Olsson A-K, Larsson H, Dixelius J, Johansson I, Lee C, Oellig C, Björk I and Claesson-Welsh L 2004 A fragment of histidine-rich glycoprotein is a potent inhibitor of tumor vascularization *Cancer Res.* **64** 599–605
[50] Pan Y, Deng L, Wang H, He K and Xia Q 2022 Histidine-rich glycoprotein (HRGP): Pleiotropic and paradoxical effects on macrophage, tumor microenvironment, angiogenesis, and other physiological and pathological processes *Genes Dis.* **9** 381–92
[51] Blank M and Shoenfeld Y 2008 Histidine-rich glycoprotein modulation of immune/autoimmune, vascular, and coagulation systems *Clin. Rev. Allergy Immunol.* **34** 307–12
[52] Zhang X, Hu W, Li J, Tao L and Wei Y 2012 A comparative study of cellular uptake and cytotoxicity of multi-walled carbon nanotubes, graphene oxide, and nanodiamond *Toxicol. Res. (Camb)* **1** 62–8
[53] Xu X, Huang B, Zeng Z, Chen J, Huang Z, Guan Z, Chen M, Huang Y and Zhao C 2020 Broaden sources and reduce expenditure: Tumor-specific transformable oxidative stress nanoamplifier enabling economized photodynamic therapy for reinforced oxidation therapy *Theranostics* **10** 10513–30
[54] Sato K, Ito K, Kohara H, Yamaguchi Y, Adachi K and Endo H 1992 Negative regulation of catalase gene expression in hepatoma cells *Mol. Cell. Biol.* **12** 2525
[55] Hasegawa Y, Takano T, Miyauchi A, Matsuzuka F, Yoshida H, Kuma K and Amino N 2002 Decreased expression of glutathione peroxidase mRNA in thyroid anaplastic carcinoma *Cancer Lett.* **182** 69–74
[56] Walkey C D, Olsen J B, Song F, Liu R, Guo H, Olsen D W H, Cohen Y, Emili A and Chan W C W 2014 Protein corona fingerprinting predicts the cellular interaction of gold and silver nanoparticles *ACS Nano* **8** 2439–55
[57] Bhowmik D, Culver K S B, Liu T and Odom T W 2019 Resolving single-nanoconstruct dynamics during targeting and nontargeting live-cell membrane interactions *ACS Nano* **13** 13637–44
[58] Lo Y L and Tu W C 2015 Co-encapsulation of chrysophsin-1 and epirubicin in PEGylated liposomes circumvents multidrug resistance in HeLa cells *Chem. Biol. Interact.* **242** 13–23
[59] Qiu N, Liu X, Zhong Y, Zhou Z, Piao Y, Miao L, Zhang Q, Tang J, Huang L and Shen Y 2016 Esterase-activated charge-reversal polymer for fibroblast-exempt cancer gene therapy *Adv. Mater.* **28** 10613–22
[60] Wang N, Chen X C, Ding R L, Yang X L, Li J, Yu X Q, Li K and Wei X 2019 Synthesis of high drug loading, reactive oxygen species and esterase dual-responsive polymeric micelles for drug delivery *RSC Adv.* **9** 2371
[61] Steichen S D, Caldorera-Moore M and Peppas N A 2013 A review of current nanoparticle and targeting moieties for the delivery of cancer therapeutics *Eur. J. Pharm. Sci.* **48** 416–27
[62] Bienert G P and Chaumont F 2014 Aquaporin-facilitated transmembrane diffusion of hydrogen peroxide *Biochimica et Biophysica Acta (BBA) - General Subjects* **1840** 1596–604
[63] Bienert G P, Schjoerring J K and Jahn T P 2006 Membrane transport of hydrogen peroxide *Biochimica et Biophysica Acta (BBA) - Biomembranes* **1758** 994–1003